Journal of Applied Polymer Science

Effect of organically modified layered double hydroxides on the properties of poly(lactic acid)/poly[(butylene succinate)-co-adipate] immiscible blends

Thobile Mhlabeni,[1,2] Sreejarani Kesavan Pillai,[1] Suprakas Sinha Ray[1,2]

[1]Centre for Nanostructures and Advanced Materials, DSI-CSIR Nanotechnology Innovation Centre, Council for Scientific and Industrial Research, Pretoria 0001, South Africa

[2]Department of Chemical Sciences, University of Johannesburg, Doornfontein 2028, Johannesburg, South Africa

Correspondence to: S. Kesavan Pillai, (E-mail: skpillai@csir.co.za)

ABSTRACT: In this study, poly(lactic acid) (PLA)/poly[(butylene succinate)-co-adipate] (PBSA) blend and its nanocomposites with layered double hydroxides (LDH) containing surface stearic acid functional groups (SaLDH) were prepared using the extrusion method, where the weight ratio of PLA/PBSA was fixed at 80/20, while that of the SaLDH varied from 0.1, 0.5, and 1.0 wt%. The characterization of SaLDH using Fourier transform infrared spectroscopy (FTIR), X-ray diffraction (XRD), and Thermogravimetric analysis (TGA) confirmed the presence of stearic acid moieties on the LDH surface. Comprehensive characterization of nanocomposites showed concurrent improvement of the thermal, mechanical, and oxygen gas barrier properties of nanocomposite containing 0.5 wt% of SaLDH. These properties are shown to result from improved interfacial interaction between the polymer matrices and the homogeneous distribution of nanoclay particles obtained at 0.5 wt% SaLDH concentration. The nanocomposite material thus shows high prospects in the industrial development of environmentally sustainable food and cosmetic packaging applications. © 2019 Wiley Periodicals, Inc. J. Appl. Polym. Sci. **2020**, *137*, 48654.

KEYWORDS: characterization; nanocomposites; PLA/PBSA blend; properties

Received 29 June 2019; accepted 4 October 2019

DOI: 10.1002/app.48654

INTRODUCTION

Polylactic lactic acid (PLA), an environmentally friendly polymer is known for its poor properties such as brittleness, which significantly limit its industrial applications, including food and cosmetic packaging. Blending with one or more other polymers serves as one of the effective and relatively cheaper routes to improve the properties of PLA.[1] However, previous studies[2–4] showed that blending PLA with more ductile biopolymers such as poly [(butylene succinate)-co-adipate] (PBSA) often forms immiscible mixtures due to unfavorable thermodynamics of mixing resulting from solubility parameters, processing temperature, and different blend compositions. The role of additional additives to improve the interfacial interaction of the polymers becomes crucial in such cases. These additives can increase the interfacial adhesion, prevent coalescence of individual polymer droplets, reduce the polymer droplet sizes, and stabilize the system more effectively, while adding other functions such as gas barrier properties (the ability to prevent the diffusion of unwanted gaseous molecules). Nanofillers such as carbon nanotubes, graphene, metal oxides, and clay nanoparticles are widely reported as additives capable of improving poor polymer properties.[5] It has been extensively demonstrated that the addition of inexpensive two-dimensional nanoclay platelets, which are of natural or synthetic origin, not only can stabilize the morphology of immiscible blend but can also significantly improve its barrier and mechanical and properties without affecting the biodegradability of the polymer matrices.[4,6,7] Therefore, a similar approach could be adopted to improve the poor oxygen gas barrier and mechanical properties of PLA/PBSA blends. The use of pristine and organically modified synthetic anionic nanoclay minerals-layered double hydroxides (LDH) have been investigated for their ability to influence the morphology and hence the properties of PLA. LDH with chemical formula $[M^{II}_{1-x}M^{III}_{x}(OH_2)]^{x+}(A^{n-}).yH_2O$ [where M^{II} -divalent metal ions (*e.g.* Mg^{2+}, Zn^{2+}, Mn^{2+}); M^{III}- trivalent metal ions (*e.g.* Al^{3+}, Fe^{3+}, Cr^{3+}); A^{n-}-anions occupying the interlayer region (*e.g.* NO_3^-, CO_3^{2-}, Cl^-); and x is the fractional aluminum substitution in the layers] has a structure similar to that of brucite ($Mg(OH)_2$).[8–10] However, unlike the brucite structure, some of the divalent metal ions are replaced with trivalent metal ions in the LDH structure. Due to the excess positive charge from the trivalent metals ions, LDH layers carry a net positive charge, which is counterbalanced

Additional Supporting Information may be found in the online version of this article.

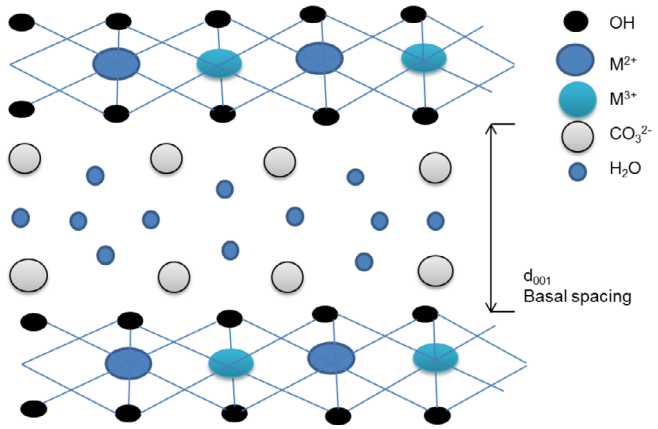

Figure 1. Chemical structure of LDH with carbonate anion in the interlayer. [Color figure can be viewed at wileyonlinelibrary.com]

by negative ions found in interlayer galleries.[8] Figure 1 is a schematic presentation of the chemical structure of LDH.

In general, it is difficult to disperse pristine LDH in polymer matrices due to its hydrophilic nature and lack of proper distribution of nanoclay platelets can negatively affect composite properties. Therefore, LDH is organically modified to improve the hydrophobicity and compatibility with the polymers. Two types of organic modifications are possible for LDH, namely surface modification, and intercalation. The former involves the adhesion of the anionic surfactant moieties on the LDH surface, and the latter through the exchange of the anionic species in the interlayer spaces of the LDH with anions of the surfactant.[11,12] Majority of the work on polymer nanocomposites reported in the literature focuses on intercalated LDH rather than surface-modified LDH. Demirkaya *et al.*,[13] prepared nanocomposite films of PLA by solution casting method using LDH intercalated with sodium dodecyl sulfate (SDS) and observed a significant decrease of the oxygen transmission rate (OTR) from 497 to 380 cm^3/cm^2.bar.day at 5 wt% clay loading in comparison to neat PLA. A subsequent study on water vapor transmission rate (WVTR) showed remarkable improvement from 278 g/m^2.day for neat PLA to 55 g/m^2.day for PLA/LDH-SDS at 5 wt%. Furthermore, LDH showed the ability to exfoliate when added to PLA, which is necessary for improved gas barrier properties. Mahboobeh *et al.*,[14,15] studied the effects of stearic acid intercalated LDH (Sa-Mg/Al LDH and Sa-Zn_3Al LDH) on the flexibility and degradation of PLA where they observed interesting morphology of the nanocomposites. The nanocomposites were prepared by solvent casting method. In the XRD analysis, the diffraction peaks of stearate-LDH were undetected and to confirm a possible exfoliated morphology, TEM analysis was also done. On the TEM images, dark lines representing LDH platelets were seen with random distribution in composites with 3, 5, 7, and 10 wt% of LDH loading. Nepalli *et al.*[16] observed a similar change in behavior of PLA after the addition of two cationic clays and anionic clay, LDH, with carbonate, stearate, palmitate anion intercalation. XRD analysis did not show any diffraction peaks corresponding to nanoclays, and however, on the TEM images, delaminated silicate platelets were seen. The addition of nanoclay particles into PLA-based matrix can result in the improvement of other characteristics such as tensile and thermal properties. Blends of PLA with other biodegradable polymers where various concentrations of organically modified natural cationic clays were used as additives have been reported earlier. Yu *et al.*[17] investigated the role of organically modified montmorillonite (MMT) clay in PLA/poly(caprolactone) (PCL) blend for the improvement of blend properties such as tensile strength, modulus, and elongation at break. Similarly, Chen and coworkers[18] investigated the effect of organically modified MMT clay and double functionalized clay on the morphology and properties of poly(l-lactic acid) (PLLA)/poly(butylene succinate) (PBS) and PLLA/PBSA blends where properties like modulus and thermal stability showed enhancement with an increase in clay loading. However, the study on the effect of organically modified (specifically the surface-modified) LDH on the properties of PLA/PBSA blend system is scarce. This work, therefore, investigated the influence of the stearic acid surface-modified layered double hydroxides (SaLDH) loading on the morphological evolution, thermal, mechanical, and oxygen gas barrier properties of PLA/PBSA/SaLDH nanocomposites. The objective of the work was to optimize the SaLDH concentration in the blend to obtain the best properties from both polymers.

EXPERIMENTAL

Materials

Commercial extrusion grade PLA (7032D) with a d-isomer content of 4% was obtained from Natureworks, LLC. PBSA BIONOLLE #3001 was obtained from Showa High Polymer (Japan). Table I shows the properties of both PLA and PBSA as per the spec sheets obtained from the manufactures. The table gives the molecular weight (Mw), density (ρ), viscosity (η_0), a glass transition (T_g), and melting temperatures (T_m). The melt flow index (MFI) for PBSA was recorded as 7 g/10 min at 210 °C, 2.16 kg load. Stearic acid surface-coated Mg-Al layered double hydroxide (SaLDH) was obtained from Hearty Chem, Korea.

Preparation of Nanocomposites

Before processing, PLA and PBSA pellets were pulverized to powder form, and then oven-dried at 80 and 60 °C, respectively, for 24 h. The dried PLA and PBSA powder form were manually mixed at a fixed ratio of 80:20 (designated as B). This ratio was selected since PLA was the primary polymer matrix and in the optimization process using 90:10, 80:20, and 70:30 PLA/PBSA blends showed improved mechanical properties at 80:20 ratio

Table I. Properties of PLA and PBSA

Material	M_w (kg/mol)	ρ (g/cm^3)	η_0 (PaS)	T_g (°C)	T_m (°C)
PLA	-	1.24	-	55–60	155–170
PBSA	190	1.23	80.8	−43.8	83.1 and 94.5

Table II. The Composition Ratio of the Prepared Nanocomposites

Nanocomposite	PLA (wt%)	PBSA (wt%)	SaLDH (wt%)
B	80	20	0
B/0.1% SaLDH	80	20	0.1
B/0.5% SaLDH	80	20	0.5
B/1.0% SaLDH	80	20	1.0

(Supporting Information Figure S1). The nanocomposites were prepared by manually mixing required quantities of SaLDH powder with the premixed dried pellets of PLA/PBSA at 80:20 ratio. The mixtures were then melt-compounded using a small-scale twin-screw extruder (Process 11, Thermo Scientific, Waltham, MA). The screw speed was set at 60 rpm and L/D was 40. The heating zones were set at a temperature range of 100–190 °C. The extrudate was used to prepare various test specimens using a Carver laboratory press (Freds. Carver Part No: 973110A) operated at 190 °C for 10 min and then cooled to room temperature. Table II shows the compositions of the prepared nanocomposites and their designations.

Characterization Techniques

FT-IR (Perkin-Elmer Spectrum 100 spectrometer) equipped with attenuated total reflection (ATR) accessory and ZnSe crystal was used to analyze the distinctive functional groups in SaLDH. The sample was mounted on the ZnSe crystal, and a force gauge between 130 and 150 N was applied. The spectrum was acquired between 550 and 4000 cm^{-1} with a resolution of 4 cm^{-1}. XRD (PANanalytical X'pertPRO diffractometer the Netherland, CuKα radiation; λ = 0.154 nm) was used to study the crystallographic structure of the nanoclay and extent of nanoclay platelets delamination in the nanocomposite materials. Circular disc samples (1.6 mm thickness × 25 mm diameter) were used for the polymer samples to obtain diffraction patterns at 45 kV (voltage) and 40 mA (current) in the 2θ diffraction angle range of 1–45° at 3.35°/min scanning speed. TEM instrument, JEOL JEM 2100 HRTEM (JEOL, Tokyo, Japan) operating at 200 kV, equipped with a Dual Vision camera from Gatan was used to study the extent of dispersion of the nanoclay platelets in the polymer matrix. Ultrathin sections (3 per sample) of the nanocomposites were prepared using Leica EM FC6 cryo-ultramicrotome (Austria) at −100 °C, cutting speed of 3 mm, and feed rate of 90 nm using a diamond knife. SEM (AURIGA CrossBeam®Workstation from Carl Zeiss, Germany) was utilized to study the surface morphology of the blend and nanocomposites. Before analysis, the samples were cryogenically fractured and subsequently subjected to coating with carbon to minimize charging. Imaging was done at an accelerating voltage of 3 kV. Thermal stability of the samples was studied using TGA (TG-Q500, TA Instruments) technique. The weight of the samples was kept in the range of 9–10 mg, and the samples were subjected to heating from 25 to 900 °C at a rate of 10 °C/min under air atmosphere. An Instron 5966 tensile tester (Instron Engineering Corporation) with a load cell of 10 kN, was used to determine the tensile strength, modulus, and elongation-at-break of the blend and nanocomposites samples according to ASTM 638D standard. This study was carried out under tension mode at a single strain rate of 5 mm/min at room temperature (25 °C). The dogbone testing specimens with dimensions of approximately 25 × 3.26 × 3.15 mm (L × W × T) were prepared by compression molding. The results presented are an average of at least five independent tests. The oxygen transmission rates (OTR) of the blend and nanocomposites were determined according to ASTM standard–D3985-02 using MOCON OX-TRAN® 2/21 MH instrument. The films for testing were prepared by compression molding. The tested area was 5 cm^2, whereas the thickness varied between 0.19 and 0.21 mm. The testing temperature was maintained at 23 °C, and the samples were conditioned for 12 h before testing. The tests were done in duplicate.

RESULTS AND DISCUSSION

Characterization of SaLDH

FTIR was used to study the functional groups of the inorganic lamellar SaLDH, its interactions with the fatty acid and the spectrum is presented in Figure 2(a). The spectrum shows a broadband ranging from 3500 to 3200 cm^{-1} representing the O—H group in the LDH structure. The robust and distinctive peak at 1369 cm^{-1} is due to the vibrations of C—O bonds attributed to the adsorbed CO_3^{2-} anions occupying the intergallery space. Zhao *et al.*,[19] observed similar results concerning the sharp carbonate peak on the FTIR study of the unmodified Mg–Al–CO_3^{2-} LDH structure. At 800 and 600 cm^{-1}, the metal-OH-metal vibrations were recorded. The C—H stretching due to the —CH_2— and —CH_3 groups of the stearic acid were observed at 2989-2866 cm^{-1}. The presence of the sharp carbonate peak suggests that the surfactants organic moieties are only on the surface of the LDH. [11] Similar results were reported in a study of flexibility improvement of PLA by stearate-modified LDH.[14]The XRD pattern [Figure 2(b)] shows a crystalline structure with a characteristic and definite peak at 2θ = 11.6 ° which corresponds to a basal spacing of 0.76–0.79 nm consistent with that of unintercalated LDH.[11] Results of XRD analysis although resembles the ordinary structure of unmodified LDH clays, the two FTIR spectral signatures of —CH_2— and —CH_3 groups show the existence of organic moieties in the sample. This result also indicates that anion exchange of CO_3^{2-} with stearate ions did not happen in the interlayer of LDH, therefore, signifying the presence of stearate anion on the surface. The TGA and corresponding derivative of TG [Figures 2(c,d)] show a three-step decomposition pattern, which can be attributed to the decomposition of physisorbed water molecules below 230 °C, dehydroxylation up to 350 °C and a combination dehydroxylation-decarbonisation reaction up to 470 °C, respectively.[12] Similar results were observed on a TGA study of stearate modified LDH.[8]

Characterization of PLA/PBSA Blend and SaLDH Nanocomposites

The Phase Structure and Morphology. Figures 3(a-d) show the phase morphologies of B and B/SaLDH nanocomposites containing various concentrations of SaLDH. From the images, it is clear that both PLA and PBSA are present in two distinct phases. The size of the PBSA droplets in blend B is comparatively bigger. This result is expected as the binary blend is made up of polymers that have high interfacial tension and the repulsion force among the polymers causes each component to remain distinct

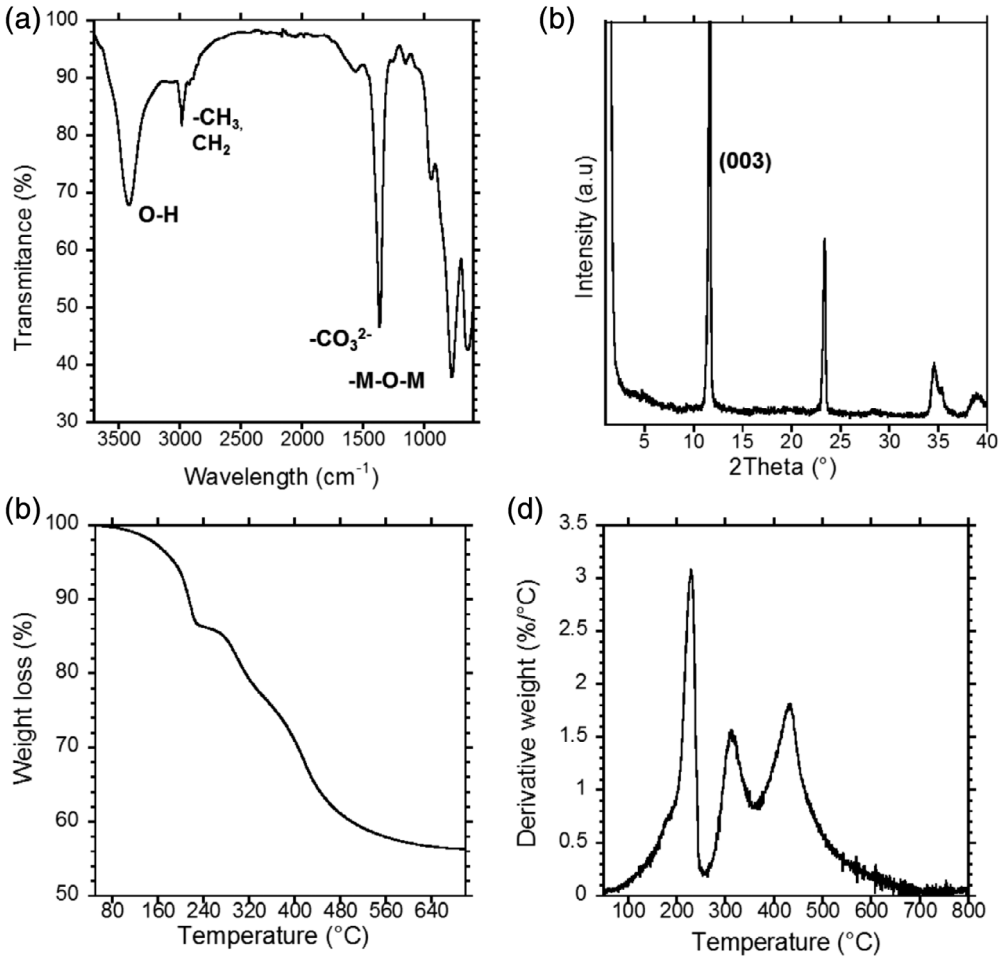

Figure 2. (a) FTIR spectrum, (b) XRD pattern, (c) TGA weight loss, and (d) derivative TG of SaLDH.

from the other. However, some interfacial interaction at the interphase of PLA and PBSA has been reported.[1–3] Among the nanocomposite samples, a significant reduction of the PBSA domain size in containing 0.5 wt% SaLDH is observed as can be seen in Figure 3(c). The reduction of the PBSA domain size is attributed to proper distribution and dispersion of clay platelets at the bulk level of the sample. At 1.0 wt% SaLDH loading the PBSA domain size shows an increase indicating the incompatibility between the blend polymer matrices. According to Ojijo *et al.*,[20] enthalpic interaction of clay particles with the polymer matrices and clay interlayer spacing play a significant role in determining the size of the dispersed PBSA phase in the blends. At lower concentration of SaLDH up to 0.5 wt%, the reduction in average PBSA droplet size establishes improved interfacial interaction between the hydrophobic surfaces of the polymers due to the presence of SaLDH clay particles in the matrix. At higher concentration, SaLDH with surfactant groups only at the surface, may not provide enough room for intercalation of both polymers at the interphase thus leading to clay aggregation and weak interaction which in turn increases the domain size of PBSA.

To further examine the dispersion of SaLDH platelets in the B matrix, high-resolution TEM analysis was carried out, and the results are presented in Figures 4(a-c). The lighter parts in the images show PLA as the continuous phase, the dispersed drop-like phase represents PBSA whereas the darker phases indicates SaLDH particles respectively. From the TEM images, it can be seen that at 0.1 wt% loading, the SaLDH particles are primarily distributed within the PBSA phase. The localization of clay particles in the PBSA phase increases as the SaLDH loading is increased to 0.5 wt%. At 1.0 wt% SaLDH concentration, an increased number of the LDH particles are observed in the PLA continuous phase as well. Ojijo *et al.*[21] obtained favored localization of organically modified cationic clays in PBSA phase in a PLA/PBSA blend with clay loading up to 1.0 wt% above which the clay particles were distributed in both polymer matrices. Mofokeng *et al.*[22] also observed the interfacial dispersion of the clay particles in polypropylene/low-density polyethylene (PP/LDPE) blend with 4.0 wt% clay loading. In both studies, the preferential localization of the clay particles was attributed to the viscosity difference of the blend's components. In an earlier study by Wu *et al.*,[23] the interfacial dispersion of functionalized multi-wall carbon nanotubes-(MWCNTs) in PCL/PLA blend was reported to contribute to the miscibility of PCL and PLA. At the processing temperature of 190 °C, PLA is found to be more viscous compared to PBSA (Supporting Information Figure S2). Hence, it is logical to assume that during the processing of the

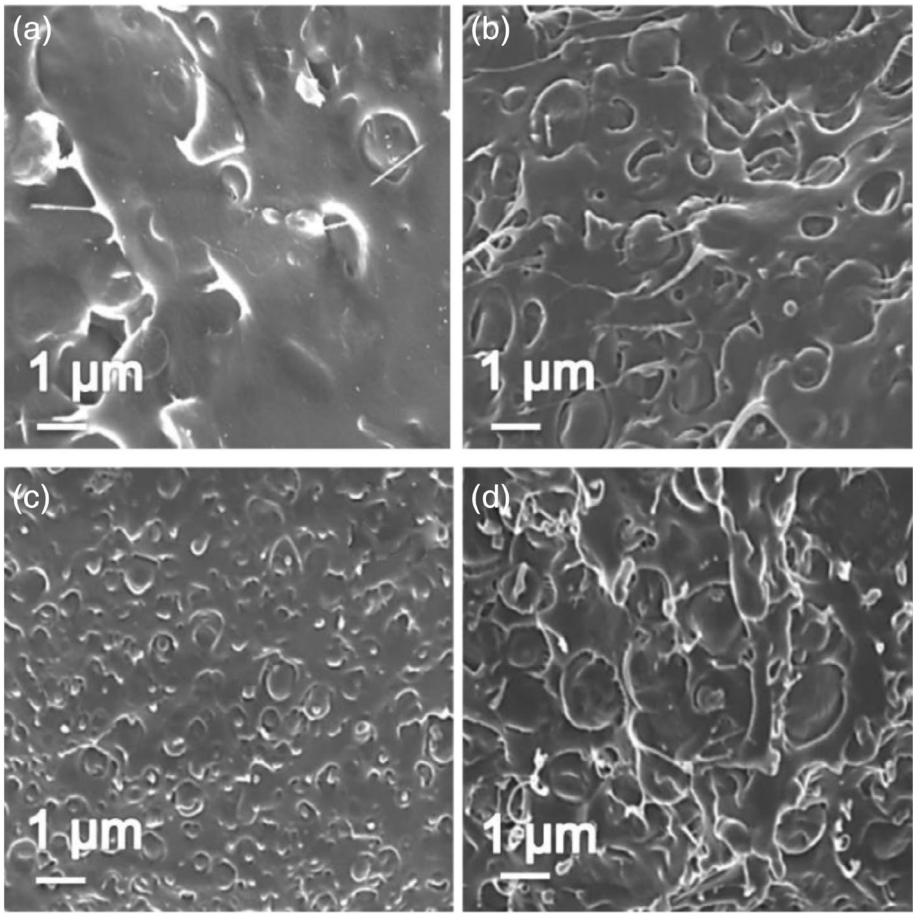

Figure 3. SEM images of the (a) B and (b) B/0.1%SaLDH, (c) B/0.5%SaLDH, and (d) B/1.0%SaLDH.

nanocomposites, the clay particles quickly get swept and mixed with the less viscous phase, PBSA, thereby increasing the viscosity of the PBSA phase. However, there is a lack of good affinity between the SaLDH and the PBSA, which could be the reason for the clay tactoids to be pushed to the interphase of PLA and PBSA. The presence of SaLDH at the interface reduces the interfacial tension between PLA and PBSA, resulting in smaller PBSA domain size as evident at 0.5 wt% SaLDH loading. Neverthless, in B/1%SaLDH, due to the presence of some clay platelets in PLA matrix, the viscosity of PLA phase also increases and hence

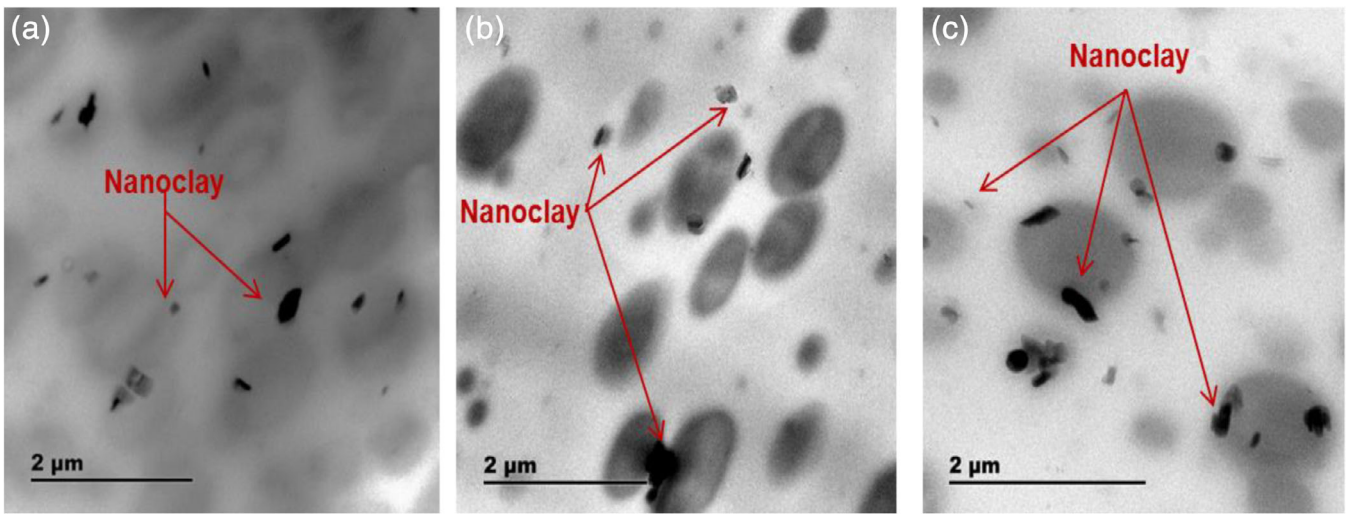

Figure 4. TEM images of (a) B/0.1%SaLDH, (b) B/0.5%SaLDH, (c) B/1.0%SaLDH. [Color figure can be viewed at wileyonlinelibrary.com]

the interfacial tension increases resulting in bigger droplet size of PBSA phase. The TEM image of B/0.1% SaLDH in Figure 4 (a) shows a relatively higher number of LDH particles, and it is possible that the imaging was done in an area with more clay particles. A comprehensive understanding of the clay particle dispersion with polymer matrix cannot be realized by the TEM image analysis due to the small area of the sample analyzed, which may not be representative of the entire sample.

The level of dispersion of SaLDH in B matrix was studied by XRD analysis, and Figure 5 shows the XRD patterns of B and B/XSaLDH nanocomposites with clay concentrations of 0.1, 0.5, and 1.0 wt%. PLA/PBSA blend did not show sharp diffraction peaks, which indicates that the structure is amorphous. In the case of nanocomposites, XRD can be employed to learn the possibly formed composite structure be it tactoid composite, intercalated, and exfoliated.[24] With tactoid composite, the primary basal peaks of the SaLDH could remain in the same position as an unmodified LDH, while in intercalated composite, the basal peaks will be still observed however at lower angles indicating increased d-spacing, whereas the exfoliated nanocomposite reveals no basal peak due to destroyed stacking of the LDH layers.[25] In the current study, the diffraction patterns of the B/0.1%SaLDH suggests that there was no ordered stacking of the LDH platelets as no crystalline peaks were observed. The absence of the diffraction peaks normally can be attributed to complete exfoliation of the LDH platelets. It might also be possible that the clay stacking was not detected during the analysis as the concentration of the clay used was very low. It is likely that X-rays hit space on the disk sample that did not have the clay platelets. Ray *et al.*[26] obtained similar results for 4.0 wt% saponite in PLA and suggested that the low silicate concentration may be a major contributing factor toward the undetected diffraction peaks. However, at SaLDH concentrations from 0.5 wt%, a small additional diffraction peak at lower 2θ value is observed left to the expected peak position of SaLDH (11.6°-indicated by the dotted line), which can be attributed to the intercalation of clay platelets with the polymer chains. XRD patterns thus give a clear indication of polymer intercalation with SaLDH at higher concentrations. These results could be considered as more reliable than TEM results as the analysis was done on a bigger sample.

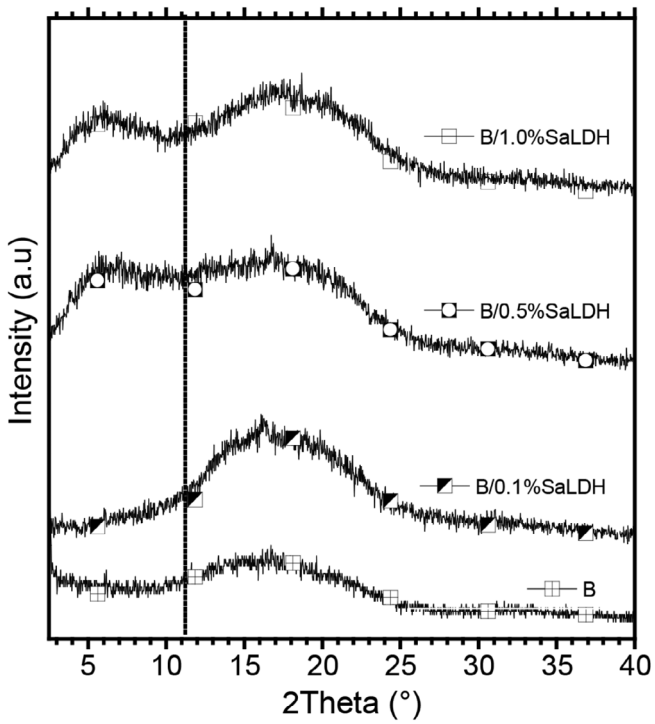

Figure 5. XRD diffraction patterns of B and B/XSaLDH nanocomposites with 0.1, 0.5, and 1.0 wt% SaLDH loading.

Mechanical Properties. Figure 6 shows the tensile modulus, strength, and elongation at break (EB) of B and B/XSaLDH nanocomposites with SaLDH concentrations of 0.1, 0.5, and 1.0 wt%. A typical stress–strain graph illustrating the type of failure occurring in the nanocomposite samples is given in Figure 6 (d). The addition of SaLDH and the increasing clay loading show a gradual increase in the modulus of the nanocomposites in comparison to the blend. This is not surprising as the increase in volume fraction of the crystalline rigid nanoparticles of high modulus is expected to stiffen the blend matrix. On the other hand, nanocomposites show an increase in tensile strength and EB, reaching a maximum at 0.5 wt% and dropping at 1.0 wt%. Al-Mulla[27] in a study on PLA/PBSA and PLA matrices with different organically modified MMT, found a slight improvement in the tensile modulus and tensile strength with the increasing concentration of the clay. In a recent study, Jamal *et al.*[28] observed a similar improvement on the tensile strength and modulus with the inclusion of sodium lauryl ether sulfate modified LDH (SLES/LDH) into PLA matrices. However, in all those studies discussed above, surfactant intercalated clays were used rather than surface-modified clays. Therefore based on the results, it is evident that the presence of surface-coated SaLDH can have a similar effect on mechanical properties of the polymer matrix as intercalated clays. This may suggest that with any organic modification, there is an optimum clay concentration that can be used, where enough clay platelets sit on the interface (as evident from the TEM result) to provide sufficient stress transfer between the two blend component polymer matrices.[29] In the current study, it is evident from the SEM and TEM results that at 0.5 wt% SaLDH, there is better interfacial interaction between PLA and PBSA, permitting more comfortable stress transfer. The bigger domain size of PBSA observed in the SEM images at 1.0 wt% SaLDH loading indicates increased immiscibility of PLA and PBSA due to possible clay aggregation. The TEM images further show an increased number of clay particles in the PLA phase at 1.0 wt% SaLDH loading leading to a mismatch of viscosity between PLA and PBSA and these two factors may result in reduced EB and tensile strength in B/1%SaLDH nanocomposite. Stress–strain curves for the samples given in Figure 6(d) show ductile fracture for B and B/XSaLDH nanocomposites. PLA is inherently brittle, (Supporting Information Figure S1) and by replacing 20% of PLA with PBSA, the ductility improves. All the nanocomposites also show a ductile fracture in which the blend containing 0.5 wt % SaLDH shows most ductility due to better interfacial interaction and load transfer between the two polymer arising from the presence of SaLDH at the interface.[1] Nanocomposites of higher SaLDH loading of 2 to 10 wt% nanocomposites were also

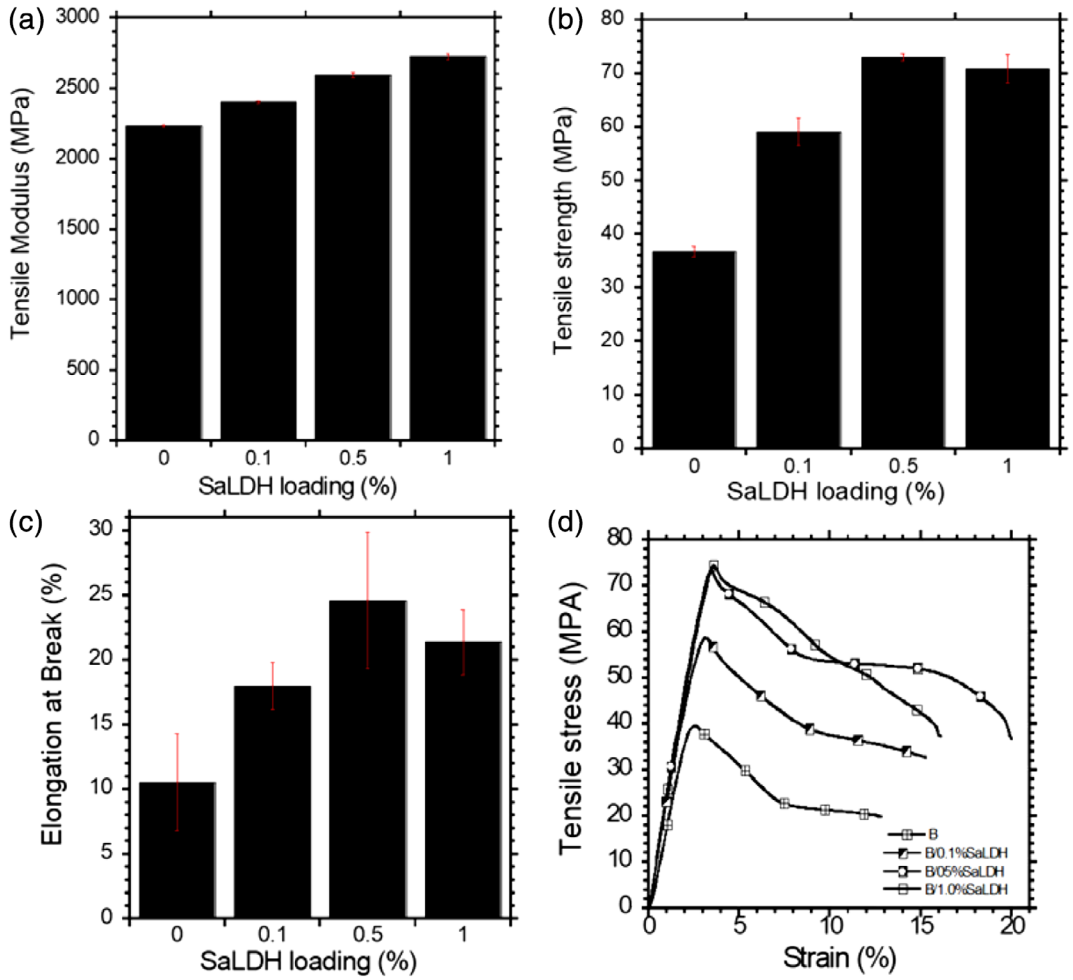

Figure 6. (a) Tensile modulus, (b) tensile strength, and (c) elongation at break, (d) typical stress–strain curves of B and B/XSaLDH with 0.1, 0.5, and 1.0 wt % of SaLDH loading. [Color figure can be viewed at wileyonlinelibrary.com]

prepared for comparison, tensile tests were done, and immediate fracture of the test specimens during the tests was observed (Supporting information Table S1).

Thermal Properties. Figure 7(a,b) show the TG weight loss and derivative TG of the B and its nanocomposites with 0.1, 0.5, and 1.0 wt% SaLDH loading, respectively. B/XSaLDH nanocomposites show a main single decomposition step associated with the degradation of the organics including the surfactant used to modify LDH occurring at the temperature range of 286–404 °C. Table III shows the average 5% decomposition temperature (T_5), 50% decomposition temperature (T_{50}), and maximum decomposition temperature (T_{max}) of the blend B and the nanocomposites B/XSaLDH with 0.1, 0.5, and 1.0 wt% SaLDH clay loading. The nanocomposite with 0.5 wt% SaLDH showed a substantial improvement in thermal stability at T_5, T_{50}, and T_{max} in comparison to 0.1 wt% SaLDH and 1.0 wt% SaLDH nanocomposites. The T_{max} peaks appear around ~370 °C for B/0.1%SaLDH and B/1.0% SaLDH and ~381 °C for B/0.5%SaLDH in both the TGA and DTG. Generally, inorganic crystalline particles have high thermal stability. As a result, it is expected that the addition of inorganic fillers, such as clays to semicrystalline polymers will improve their overall thermal stability. High interfacial interaction between the clay particles and the host polymers can also contribute to the overall thermal stability of the nanocomposite, which may be the case at 0.5 wt% SaLDH clay loading. In a study by Paula *et al.*,[30] it was demonstrated that the clay particles reinforced the polymer by immobilizing the polymer chains. Studies suggest that clay inorganics increase heat diffusion path and slow down the process of combustion, thus enhancing the thermal stability of nanocomposites.[31] MMT modified with various surfactants obtained the desired interfacial interactions with PLA, and it resulted in the improvement of thermal stability.[32,33] In this study, the thermal stability at T_5, T_{50}, and T_{max} of the nanocomposites is relatively lower at 0.1 wt% SaLDH and 1.0 wt % SaLDH when compared to 0.5 wt% SaLDH loading. As suggested by SEM images and mechanical properties, 0.5 wt% may be an optimum concentration SaLDH required for better interfacial interaction to realize an improvement in thermal stability. More uniform clay dispersion at 0.5 wt% SaLDH can result in the more homogenous surface for sufficient heat transfer thereby improving the thermal stability of the nanocomposite. A study by Ojijo *et al.*[34] based on PLA and MMT (Cloisite C20A) with different clay loadings of 0.5, 1, 2, 4, 6, and 9 wt% reported

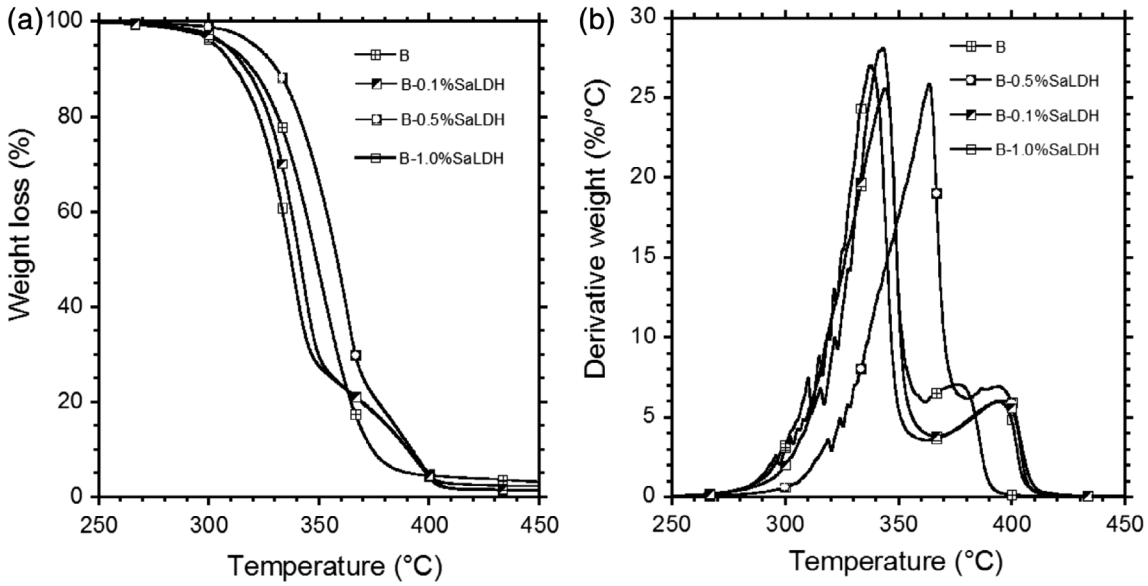

Figure 7. (a) TGA weight loss and (b) derivative TG of the blend B and B/XSaLDH with 0.1, 0.5, and 1.0 wt% clay loading.

Table III. Thermal Properties of B and B/XSaLDH With 0.1, 0.5 and 1.0 wt% SaLDH Loading

Sample	T_5 (°C)	T_{50} (°C)	T_{max} (°C)
B	307 ± 0.35	340 ± 0.53	344 ± 0.28
B/0.1%SaLDH	308 ± 0.28	342 ± 0.65	342 ± 0.52
B/0.5%SaLDH	320 ± 0.53	358 ± 4.24	363 ± 0.35
B/1.0%SaLDH	302 ± 0.72	337 ± 1.00	337 ± 0.53

similar results with regards to optimum clay concentration. In the study, they showed a slight improvement in the thermal stability up to 2 wt% whereas a decrease in thermal stability was observed from 4 to 9 wt% clay loading. Three factors that may contribute to the thermal stability were proposed; the concentration of clay, dispersion of clay particles within the polymer matrix, and the resulting structure of the nanocomposites. Interestingly, Chang *et al.*[35] did not observe an optimum clay concentration that resulted in superior thermal stability in a study of PLA/C16-MMT with clay concentrations of 2, 4, 6, and 8 wt%. However, they observed a decreasing trend in thermal stability with increasing clay loading. No inference was provided as to why there was reduced thermal stability with the increasing clay content in their study.

Oxygen Gas Barrier Properties. Table IV shows the thickness normalized oxygen transmission rate (OTR) of blend B and B/XSaLDH nanocomposites. The OTR oxygen transmission rate of B is 45.1 g/m^2.day. The nanocomposites have comparatively lower OTR, where the OTR decreases to 40.1, 35.5, and 37.9 g/m^2.day for B/0.1%SaLDH, B/0.5%SaLDH and B/1.0%SaLDH, respectively. A simplified permeability model proposed by Neilsens suggests that the presence of layered inorganic structures reduces the diffusion of gaseous molecules through the nanocomposites due to the impermeable crystalline structure of clay platelets resulting in a tortuous pathway for the gas molecules.[36–39] From the results, it is apparent that the incorporation of SaLDH improves oxygen gas barrier property (inverse relation between barrier property and OTR) of the blend B gradually up to SaLDH loading of 0.5 wt% and after that begin to reduce. Li *et al.*[40] studied oxygen barrier of poly(propylene carbonate) (PPC)/1%organically modified LDH (OLDH), PPC/2% OLDH, and PPC/3%OLDH, and it was observed that OTR decreased with increasing clay content up to 3.0 wt% and after that started to increase. Bhatia *et al.*[41] also found a similar decreasing trend of OTR with increasing clay content for PLA/PBS/MMT (Closite 30B). Factors such as clay platelet aspect ratio, clay concentration, and dispersion of clay particles play a significant role in determining the diffusion rate of gas molecules. In this study, the nanocomposites were prepared using the same clay, which then eliminates the effect of aspect ratio. This leaves

Table IV. OTR of Blend B and B/XSaLDH With 0.1, 0.5, and 1.0 wt% Clay Loading

Samples	OTR (g/m^2.day)	Average thickness (mm)
B	45.1 ± 0.12	0.214 ± 0.01
B/0.1%SaLDH	40.1 ± 0.09	0.184 ± 0.01
B/0.5%SaLDH	35.5 ± 0.06	0.192 ± 0.00
B/1.0%SaLDH	37.9 ± 0.08	0.202 ± 0.00

the clay concentration and extent of clay dispersion in the polymer matrices as the major contributing factors to the oxygen molecules transmission rate through the nanocomposite films. Although XRD analysis suggested possible intercalation of clay platelets at B/0.5%SaLDH and B/1.0%SaLDH nanocomposites, further characterization on the morphological, mechanical, and thermal properties of the nanocomposites revealed good SaLDH dispersion and interfacial interaction in nanocomposite only at 0.5 wt% loading. The lowest OTR (20.3% lower than the neat blend) and the improved oxygen barrier property obtained for B/0.5% SaLDH is therefore in agreement with proper clay distribution resulting in reinforced structure and homogeneous morphology of the composite.

CONCLUSIONS

The nanocomposites of PLA/PBSA and SaLDH show that the presence of surface surfactant groups of organically modified LDH can bind with the polymer matrix resulting in concurrent improvement in mechanical, thermal, and barrier properties of the nanocomposite. Surface-modified LDH particles might produce a similar effect as surfactant intercalated counterparts at a relatively much lower concentration. The analysis of the results provides conclusive evidence that at 0.5 wt% SaLDH loading, optimum properties can be realized. The difference in viscosity between PLA and PBSA is found to influence the preferential localization of SaLDH in the blend matrix significantly. B/0.5%SaLDH nanocomposite shows the ability to endure higher stress applied before it undergoes deformation and hence demonstrates the ability to elongate better. Furthermore, the uniform distribution of clay particles at the 0.5 wt % SaLDH loading resulted in the overall thermal stability and reduced diffusion rate of oxygen molecules. The improved barrier property against oxygen transmission, thermal property, and increased elongation at break at optimal clay loading suggests great prospects of these blend nanocomposites in the application of sustainable food and cosmetic packaging.

ACKNOWLEDGMENTS

This work was supported by the National Research Foundation (Grant No. 111229) in collaboration with the Department of Science and Technology and the Council for Scientific and Industrial Research (National Centre for Nanostructured Materials).

REFERENCES

1. Ojijo, V.; Ray, S. S.; Sadiku, R. *Appl. Mater. Interfaces.* **2012**, *4*, 6690.
2. Lee, S.; Lee, J. W. *Korea-Aust. Rheol.* **2005**, *17*(2), 71.
3. Pivsa-Art, W.; Pivsa-Art, S.; Fujii, K.; Nomura, K.; Ishimoto, K.; Aso, Y.; Yamane, H.; Hitomi Ohara, H. *Appl. Polym. Sci.* **2015**, *41856*, 1.
4. Ojijo, V.; Ray, S. S.; Sadiku, R. *Appl. Mater. Interfaces.* **2013**, *5*, 4266.
5. Stefanescu, E. A.; Daranga, C.; Stefanescu, C. *Mater.* **2009**, *2*, 2095.
6. Rhima, J.-W.; Park, H.-M.; Ha, C.–. S. *Prog. Polym. Sci.* **2013**, *38*, 1629.
7. Bikiaris, D.; Polym, N. *Degrad. Stab.* **1908**-1928, *2013*, 98.
8. Focke, W. W.; Nhlapo, N. S.; Moyo, L.; Verryn, S. M. C. *Mol. Cryst. Liq. Cryst.* **2010**, *521*, 168.
9. Newman, S. P.; Jones, W. *New J. Chem.* **1998**, *22*, 105.
10. Mosangi, D.; Moyo, L.; Pillai, S. K.; Ray, S. S. *Royal Soc. Chem.* **2016**, *6*, 105862.
11. Moyo, L.; Nhlapo, N.; Focke, W. W. *J. Mater. Sci.* **2008**, *43*, 6144.
12. Wang, J.; Stevens, L. A.; Drage, T. C.; Wood, J. *Chem. Eng. Sci.* **2012**, *68*, 424.
13. Demirkaya, Z. D.; Sengul, B.; Eroglu, M. S.; Dilsiz, N. *J. Polym. Res.* **2015**, *22*, 1.
14. Mahboobeh, E.; Yunus, W. M.; Hussein, Z.; Ahmad, M.; Ibrahim, N. A. *Appl. Polym. Sci.* **2010**, *118*, 1077.
15. Mahboobeh, E.; Shameli, K.; Ibrahim, N. A.; Yunus, W. M. *Inter. J. Mol. Sci.* **2012**, *13*, 7938.
16. Neppalli, R.; Causin, V.; Marega, C.; Modesti, M.; Adhikari, R.; Scholtyssek, S.; Ray, S. S.; Marigo, A. *Appl. Clay Sci.* **2014**, *87*, 278.
17. Yu, Z.; Yin, J.; Yan, S.; Xie, Y.; Ma, J.; Chen, X. *Polym.* **2007**, *48*, 6439.
18. Chen, G.–. X.; Kin, H.–. S.; Kim, E.–. S.; Yoon, J.–. S. *Polym.* **2005**, *46*, 11829.
19. Zhao, N.; Shi, S.; Lu, G.; Wei, G. J. *Phys. Chem. Solids.* **2008**, *69*, 1564.
20. Ojijo, V.; Cele, H.; Ray, S. S. *Macromol. Mater. Eng.* **2011**, *296*, 865.
21. Ojijo, V.; Malwela, T.; Ray, S. S.; Sadiku, R. *Polym.* **2012**, *53*, 505.
22. Mofokeng, T. G.; Ray, S. S.; Ojijo, V. *Appl. Polym. Sci.* **2018**, *46193*, 1.
23. Wu, D.; Zhang, Y.; Zhang, M.; Yu, W. *Biomacromolecules*. **2009**, *10*, 417.
24. Chen, B.; Evans, J. R.; Greenwell, C. H.; Boulet, P.; Coveney, P. V.; Bowden, A. A.; Whiting, A. *Royal Soc. Chem.* **2008**, *37*, 568.
25. Duncan, T. V. J. *Colloid. Interface. Sci.* **2011**, *363*, 1.
26. Ray, S. S.; Yamadab, K. O.; Fujimoto, Y.; Ogami, A.; Uedab, K. *Polym.* **2003**, *44*, 6633.
27. Al-Mulla, E. A. *Fibers Polym.* **2011**, *12*(4), 444.
28. Jamal, S. H.; Khim, O. K.; Kasim, N. A.; Ahmad, M.; Yunus, W. M.; Inter, J. *Adv. Appl. Sci.* **2017**, *4*(12), 100.
29. Al-Itry, R.; Lamnawar, K.; Maazouz, A. *Polym. Degrad. Stab.* **2012**, *97*, 1898.
30. Paula, M. -A.; Alexandre, M.; Degeé, P.; Henrist, C.; Rulmont, A.; Dubois, P. *Polym.* **2003**, *44*, 443.
31. Zanetti, M.; Camino, G.; Mulhaupt, R. *Polym. Degrad. Stab.* **2001**, *74*(3), 413.
32. Thellen, C.; Orroth, C.; Froio, D.; Ziegler, D.; Lucciarini, J.; Farrell, R.; D'Souza, A. N.; Ratto, J. A. *Polym.* **2005**, *46*, 11716.
33. Lin, L.-H.; Liu, H.-J.; Yu, N.-K. *Appl. Polym. Sci.* **2007**, *106*, 260.

34. Ojijo, V.; Ray, S. S.; Sadiku, R. *Appl. Mater. Interfaces.* **2012**, *4*, 2395.
35. Chang, J.-H.; An, Y. U.; Sur, G. S. *Polym. Sci. Part B: Polym. Phys.* **2003**, *41*, 94.
36. Neilsen, L. E. J. *Macromol. Sci.* **1967**, *5*, 929.
37. Maiti, P.; Yamada, K.; Okamoto, M.; Ueda, K.; Okamoto, K. *Chem. Mater.* **2002**, *14*, 4654.
38. Sabet, S. S.; Katbab, A. A. *Appl. Polym. Sci.* **2009**, *111*, 1954.
39. Ray, S. S.; Okamoto, M. *Prog. Polym. Sci.* **2003**, *28*, 1539.
40. Li, G.; Luo, W.; Xiao, M.; Wang, S.; Meng, Y. *Chin. J. Polym. Sci.* **2016**, *34*(1), 13.
41. Bhatia, A.; Gupta, R. K.; Bhattacharya, S. N.; Cho, H. *J. Inter. Polym. Proc.* **2010**, *1*, 5.